Venus and its ionosphere

Hari Om Upadhyay* and R. N. Singh**

Department of Physics, Banaras Hindu University, Varanasi 221 005, India
* Present address National Physical Laboratory, K. S Krishnan Marg, New Delhi 110 012, India
** Department of Applied Physics, Institute of Technology, Banaras Hindu University, Varanasi 221 005, India

In this article the formation of Venus ionosphere has been studied on a line similar to that followed for the study of Earth's ionosphere. The neutral density of Venusian gases, their solar activity dependence and variation with solar Zenith angle have been modelled. The EUV solar flux data are similar to that used for modelling Earth's ionosphere. The solar flux incident on Venus has been enhanced following the inverse square radial distance variation. Considering the incidence of changed solar flux on the Venus atmospheric constituents and selecting appropriate ionization and absorption cross-sections for ambient neutral gases, the electron–ion pair production rates have been computed. The electron–ion kinetics has been used extensively and dominant reaction rates have been used for computing the steady state ion density and electron density height profiles in the altitude range of 100–800 km. It is shown that the ion densities and electron density below 250 km compare well with the theoretical results reported by other workers and the *in situ* measurements made by OIMS (Orbiter Ion Mass Spectrometer) aboard PVO. However, we find that the theoretically computed results above 250 km are considerably large. This is likely to arise due to the presence of transport processes which is responsible for dynamic equilibrium processes and redistribution of electron and ion densities in the upper part of the Venus atmosphere. The detailed transport processes in the Venus upper atmosphere are not yet fully known, therefore, in the present modelling we have not included the effect of transport processes. The results of modelling are discussed in the light of known transport processes which are similar to that of Earth's atmosphere.

THE complete knowledge of the neutral atmosphere, its dependence on temperature, pressure and magnetic field distribution with altitude are essential for modelling of ionization in any planetary atmosphere. The effect of external sources such as Sun's electromagnetic radiations, solar wind interaction and changes with solar activity can be best understood when the intrinsic atmospheric details are well known. The processes of Earth's ionosphere formation are well known. Study of Venus ionospheric formation has been carried out by many workers[1–3]. The availability of *in situ* measurements by various probes aboard Pioneer Venus Orbiter (PVO) has inspired a fresh theoretical modelling and comparison with directly measured data over a long period of time. The choice of Venus neutral atmosphere and solar flux has been made. Using the neutral gas density model, spectral features of solar EUV flux[4] and relevant cross-sections[5–7], we have computed the electron–ion pair production rate in accordance with the photoionization theory as used by earlier workers[1, 8]. The ion-kinetics taking place into the ionosphere governs the production and loss of photoions and also governs the existence of steady state electron and ion densities. The steady state electron and ion densities are dependent on the choice of various input parameters. Therefore, ionospheric models for various solar activity periods have been computed which accounts for changes in neutral densities corresponding to solar flux changes. The nature of variations of ion densities and electron densities measured by different planetary flybys and orbiter missions have been collected and the computed results are compared; similarities and discrepancies are discussed.

Ionizing solar flux models

The Sun for many purposes is considered to be a constant source of electromagnetic wave radiation characterized by a fixed value of the solar constant. However, on various long and short time scales, the Sun is known to exhibit interesting changes in some of the observed electromagnetic wave and corpuscular emissions. The eleven-year solar cycle variations are one of the most important long term effects which depicts cyclic variation of sunspot number. The maximum of the sunspots number are extensively used to classify the part of the solar cycle as solar maximum period and the low sunspots number as solar minimum period. These features are known to recur and accordingly affect the atmospheric neutral density of the planetary atmosphere, and in turn also govern the ionization density distributions with altitude.

The XEUV emissions and microwave radiations during the solar flare, when monitored from the ground-based stations, are found to change due to the presence of cloud top and other simultaneously occurring atmo-

Table 1. Solar UV flux data UV spectrum from 50 to 1050 Å intensity incident on earth (10^9 photons cm^{-2} sec^{-1})

Solar flux period	ION	76200 Model-I	78348 Model-II	79050 Model-III
Wavelength (Å)				
50–200		0 4382	1 0337	1 3710
100–150		0.1687	0 3623	0 4675
150–200		I 8692	4 1772	5 7024
200–250		1 3951	4 7953	7.1448
256 3	He II, Si X	0.5064	0 8805	1 0832
284 15	Fe XV	0 0773	3 2613	5.7229
250–300		1.3556	7.5081	12 1600
303 31	Si XI	0 6000	2 9100	4 6908
303 78	He II	7 7625	12 3424	14 3956
300–350		0 8671	4.3119	6 8315
368 7	Mg IX	0.7394	1 2891	I.5355
350–400		0 2121	I 5298	2.5423
400–450		0.4073	1.0922	1 5310
465 22	Ne VII	0.3299	0 6102	0.7358
450–500		0.3081	1 2120	1.8228
500–550		0 5085	1.2303	1 6486
554 37	O IV	0.7992	1 2943	1 5163
584 33	He I	1 5875	3 4608	4 3005
550–600		0 4843	0 8732	1 0477
609 76	Mg X	0 6333	1 67g2	2 4838
629 73	O V	1 8484	3 2443	3 8701
600–650		0 4002	0 9606	1 3672
650–700		0.2623	0 4521	0.5388
703 31	O III	0 3915	0 6363	0 7461
700–750		0.1667	0.3439	0 4287
765 15	N IV	0 1997	0 3647	0.4386
770 41	Ne VIII	0.2425	0 7760	I 1873
789 36	O IV	0 7831	1 2870	1 5140
750–800		0 8728	1 8909	2 4541
800–850		1 9311	3 9278	4 8538
850–900		4 4325	9 7798	12.2187
900–950		3 6994	7 9445	9 8513
977 02	C III	4 8400	8 5523	10.2165
950–1000		1 7155	3.3468	4 0779
1025.72	H I	4 3750	9 5375	11 8519
1031 91	O VI	1.9425	4 2929	6 1049
1000–1050		2 4775	4 7145	6 0928
Sunspot number		0	140	166
$F_{10\ 7}$ daily*		70 06	192.7	237 8
$F_{10\ 7}$ 27 days average		68 0	206 0	243 0
$F_{10\ 7}$ 81 days average		71 3	174 3	197 0

*$F_{10\ 7}$ is in units of 10^{-22} Wm^{-2} Hz^{-1}.

spheric effects. The microwave radiation at 2800 MHz (10.7 cm) reaches the planetary atmospheres almost unattenuated and is extensively used to classify the effect of solar activity. These solar activity indices have been used to study the variations induced in the neutral density composition of the planetary atmospheres[9]. These radiations take account of comparatively short term variations to depict the effect of 27-day solar rotation on planetary atmospheres. To obtain the theoretical estimates of the electron density profiles and compare them with *in situ* measured electron density profiles, it is important to know the exact radiations of the solar XEUV fluxes and their variations with changing values of 10.7 cm fluxes. Whenever exact solar flux data for different solar activity periods are not available, some type of solar flux modelling is made to study its effect. In such cases, two key wavelengths (Fe XVI-335 Å coronal and HI lyman β 1025.7 Å – chromospheric) together with some scaling coefficients are generally used to obtain the nature of variations in the extended region of solar EUV spectrum[10]. In the present study, we have used measured solar flux data corresponding to different solar activity periods as shown in Table 1. Three solar EUV flux models have

been chosen which correspond to increasing values of 10.7 cm flux. The solar EUV flux for Model-I is comparatively small compared to Models-II and III. There is no general and consistent factor by which one solar flux model differs from another solar flux model. We find that in each wavelength band the factor of solar flux enhancement changes in the three models used in this study.

Modelling of the neutral atmosphere

The neutral constituents of the Venus atmosphere are known to change with solar activity as a result of differential heating of the Venus atmosphere. The steady state neutral density height profiles are established as a consequence of competing processes of particle diffusion and escape of neutral particles from the planetary atmospheres. Without going into the details of exact transport processes, we have only adopted a model for changes in the density of various neutral constituents of Venus atmosphere. The absolute neutral density profiles are therefore obtained by indirect *in situ* measurements. Different types of measurements are made and neutral density models are prepared by synthesizing various *in situ* measurements. The models thus prepared, account for the pre-ionized neutral gas density variations with solar activity in the Venus atmosphere.

In order to account for neutral gas density changes as a function of solar activity index, we have used a simplified empirical model for the change in neutral gas number density n_n as given by Kliore *et al.*[9]

$$\log_{10} n_n = A + B + 0.44\, m_n [(\Delta T_{\infty,s} + \Delta T_{\infty,L})/T^2](Z - 150), \quad (1)$$

where T is the ambient temperature, m_n the molecular weight, Z the altitude in km above Venus radius 6052 km, $\bar{F}_{10.7}$ the 81-day mean of 10.7 cm solar flux at 1 AU divided by 10^{-22} Wm^{-2} Hz^{-1}; and $F_{10.7}$ the daily value of 10.7 cm solar activity index at 1 AU (determined for the direction of Venus taking into account a 27-day rotation of the Sun) divided by 10^{-22} Wm^{-2} Hz^{-1}.

The subscript n used in equation (1) denotes the neutral atmospheric species. The variations of A, $\Delta T_{\infty,L}$ as function of $\bar{F}_{10.7}$ and B, $\Delta T_{\infty,s}$ with $(F_{10.7} - \bar{F}_{10.7})$ have been shown with the help of nomograms in Figure 1 *a* and *b* respectively. Using this empirical formula, we have prepared the neutral density height profiles variation with solar activity indices for studying the photoionization and computing the corresponding steady state electron density profiles and these profiles are shown in Figure 2.

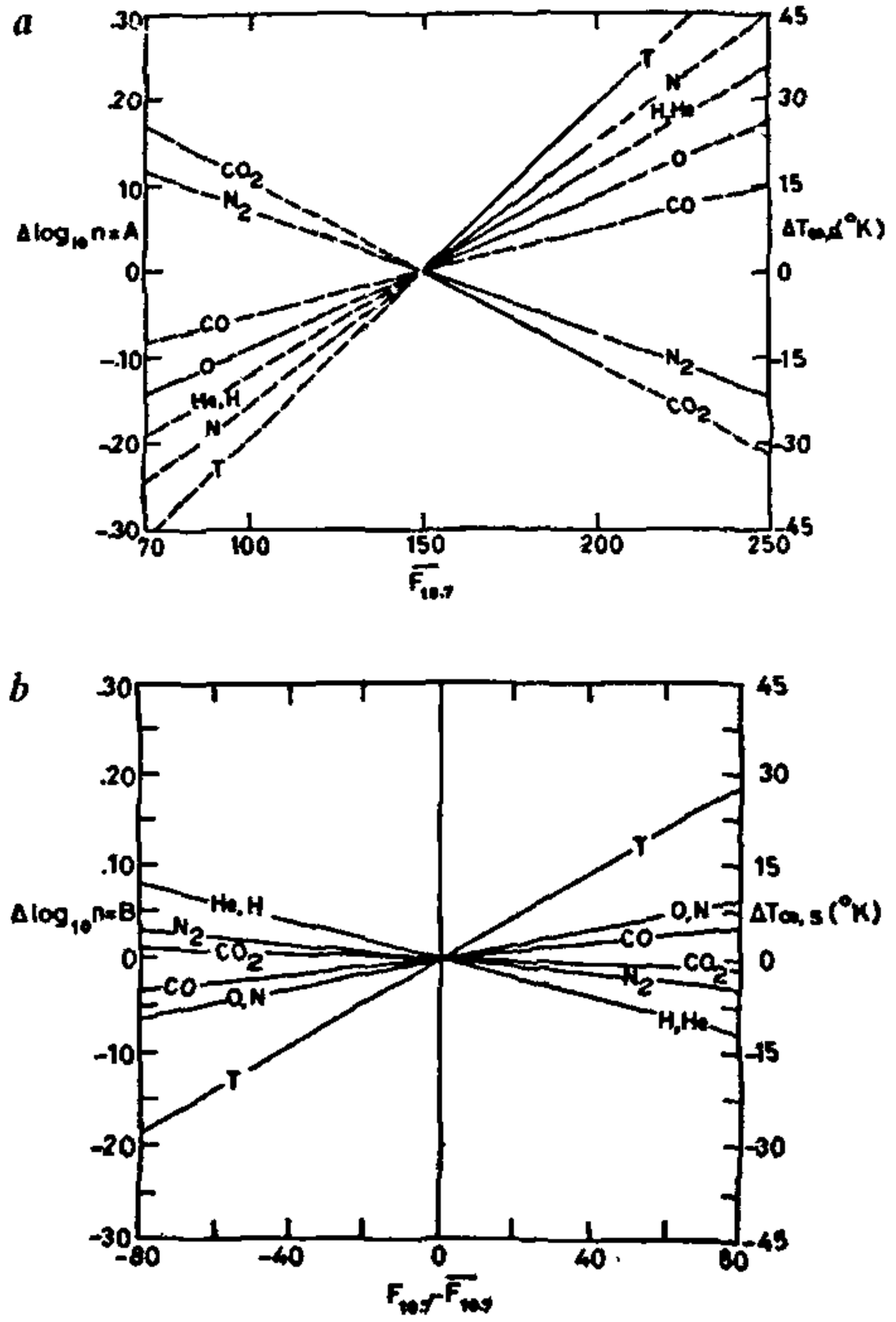

Figure 1 *a* and *b*. *a*. Long-term response of atmosphere to $F_{10.7}$ index (A and $\Delta T_{\infty,L}$ are defined in the text) *b*. Short-term response of atmosphere to $F_{10.7}$ index variations from $\bar{F}_{10.7}$ (B and $\Delta T_{\infty,s}$ are defined in the text).

Theory of photoionization

The electron–ion pair production rate in the Venus atmosphere has been computed using widely used photo-ionization theory[3]. The electron–ion pair production rate is written as

$$q_n(Z,\chi) = n_n(Z) \int_0^\infty d\lambda\, I_\infty(\lambda)\sigma_n^{(i)}(\lambda)\exp[-\tau(\lambda,Z)], \quad (2)$$

where $n_n(Z)$ is the number density of neutral gas constituents as function of height (Z), $\sigma_n^{(i)}(\lambda)$ the ionization cross-section of nth constituents as a function of wavelength, $I_\infty(\lambda)$ the spectrum of solar radiation incident upon the top of the ionosphere.

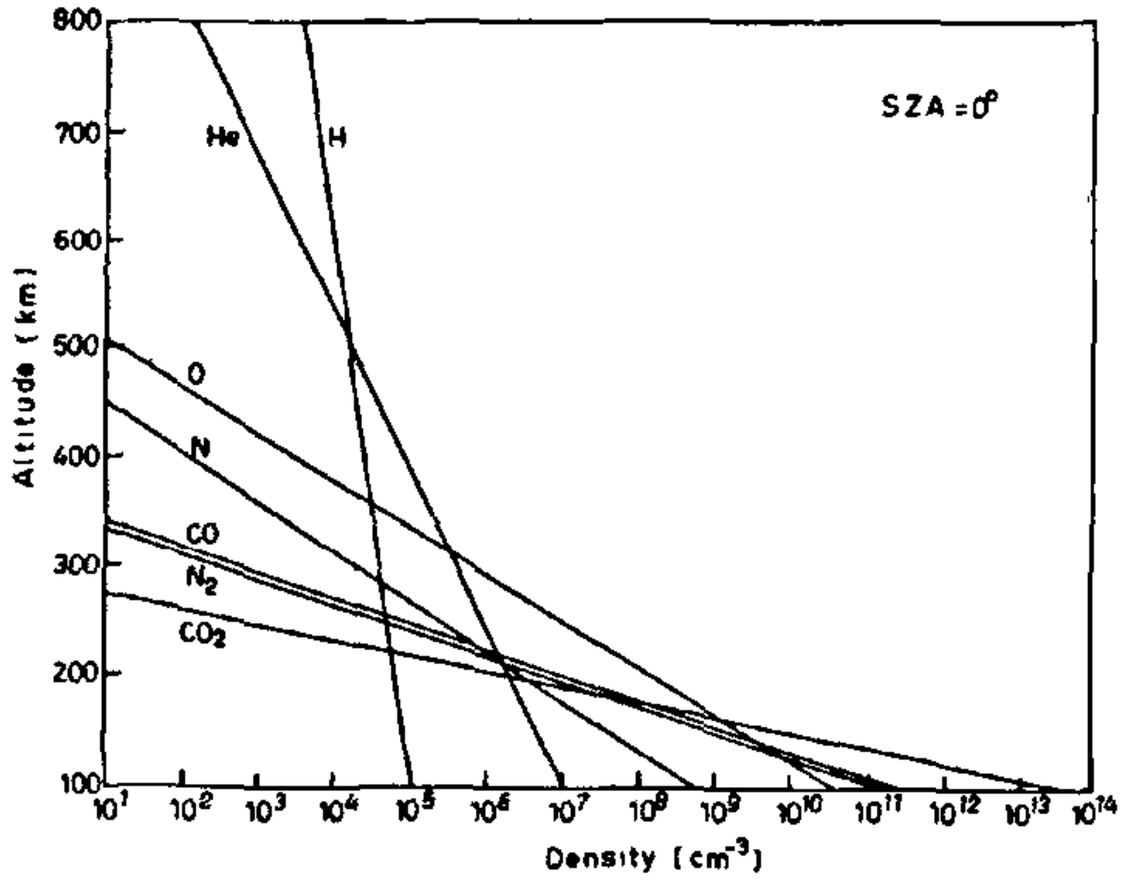

Figure 2. VIRA model (100–800 km. SZA = 0°) for neutral density of Venus atmosphere (results for higher altitudes have been extrapolated)

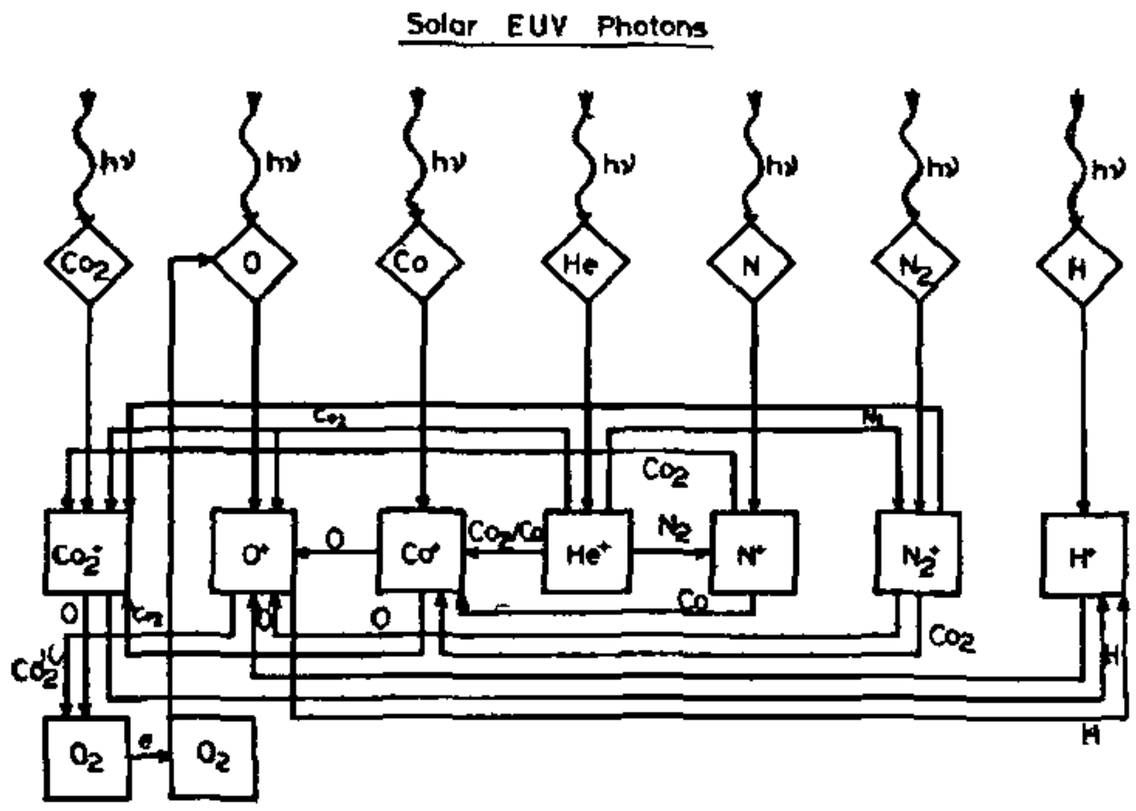

Figure 3. Flow diagram of the major ion chemistry scheme used in the computation of ion density profiles in Venus ionosphere

The optical depth of the atmosphere is defined as

$$\tau(\lambda, Z) = \sum_n \sigma_n^{(a)}(\lambda) n_n(Z) H_n(Z) \mathrm{Ch}(R_n, \chi), \qquad (3)$$

where $R_n = \left(\frac{R+Z}{H_n(z)}\right)$, R being radius of Venus in km, χ the solar zenith angle (SZA), $H_n(Z)$ the scale height $(KT_n / m_n g)$ and $\mathrm{Ch}(R_n, \chi)$ the Chapman grazing incidence function. We have used these values from tables of Wilkes[11] and approximate expression valid for both large and small SZA presented by Smith and Smith[12]. For $\chi < 82°$ the Chapman function has been replaced by Sec χ in the summation of equation (3).

Ionospheric chemistry

There are myriads of chemical reactions that are potentially important in the Venus ionosphere. A summary of the most important ion-neutral reactions and dissociative recombination rates are given in Table 2 (refs. 1, 8) along with the best available values of these rate coefficients. A scheme of chemical reactions in the Venus ionosphere is shown in Figure 3. The ion-chemistry dominating the CO_2^+, O^+, CO^+, He^+, N^+, N_2^+, H^+ and O_2^+ abundance in the chemically controlled region (which is in the altitude range extending up to 200 km) of the Venus ionosphere has been illustrated. It is obvious from Figure 3 that the primary ions, CO_2^+ and O^+ undergo various ionic reactions with the different reactions rates (R1, R8) and are rapidly transformed into O_2 which is the dominant ion in certain regions of the Venus ionosphere. Reactions involving metastable species are not listed in Table 2, and authentic data are not yet available. However, Fox[13] has shown that some of the metastable reactions do play an important role in the chemistry of some of the observed ionic species, and their inclusion in the computation of steady state ion density and generated optical emission improve the agreement between the observed and calculated values of electron and ion density height profiles and optical emissions.

Chemical reactions and equilibrium ion electron density

The ions produced by photoionization processes further interact with the neutral gases and charged particles and a fraction of these is lost in the process. The important processes for the loss of ions are dissociation, recombination, charge-exchange and ion interchange. The lifetime or abundance of ions in the Venus ionosphere depends on the rate coefficients of various reactions which play an important role in controlling the ion and electron densities in the Venus ionosphere. In the absence of detailed information, one has to compromise with the limited information in an effort to prepare the theoretical model. Keeping this in view, we have included all major production and loss reactions whose variations significantly affect the modelling results. We have ignored many reactions which are believed to be of secondary importance or whose rate coefficients are not yet precisely known. Including all possible reactions would indeed turn out to be very unwieldy, costly and a time-consuming effort without improving the results very significantly. The continuity equation is written for either positive and negative ion or, indeed, for any one of the constituents whose concentration is subject to change within a cell of unit volume. The temporal

Table 2. Ion-neutral reaction rates

Reaction number	Reaction	Rate constants $cm^3\ sec^{-1}$
R1	$CO_2^+ + O \rightarrow O_2^+ + CO$	1.6×10^{-10}
R2	$CO_2^+ + H \rightarrow H^+ + CO_2$	1.0×10^{-10}
R3	$CO^+ + O \rightarrow O^+ + CO$	1.4×10^{-10}
R4	$CO^+ + CO_2 \rightarrow CO_2^+ + CO$	1.0×10^{-9}
R5	$N_2^+ + CO \rightarrow CO^+ + N_2$	7.4×10^{-11}
R6	$N_2^+ + CO_2 \rightarrow CO_2^+ + N_2$	7.7×10^{-10}
R7	$N_2^+ + O \rightarrow O_2^+ + N_2$	$3.6 \times 10^{-12} \times (Te/300)^{0.41}$
R8	$O^+ + CO_2 \rightarrow O^- + CO$	1.2×10^{-9}
R9	$O^+ + H \rightarrow H^+ + O$	$2.5 \times 10^{-11} \times T_n^{1/2}$
R10	$N^+ + CO \rightarrow CO^+ + N$	4.0×10^{-10}
R11	$N^+ + CO_2 \rightarrow CO_2^+ + N$	7.5×10^{-10}
R12	$He^+ + CO_2 \rightarrow CO^+ + O + He$	8.7×10^{-10}
R13	$He^+ + CO_2 \rightarrow CO_2^+ + He$	1.2×10^{-10}
R14	$He^+ + CO_2 \rightarrow O^+ + CO + He$	1.0×10^{-10}
R15	$He^+ + CO \rightarrow CO^+ + He$	1.68×10^{-9}
R16	$He^+ + N_2 \rightarrow N^+ + N + He$	9.6×10^{-10}
R17	$He^+ + N_2 \rightarrow N_2^+ + He$	6.4×10^{-10}
R18	$H^+ + O \rightarrow O^+ + H$	$2.2 \times 10^{-11} \times T_i^{1/2}$
	Dissociative recombination rates	
A1	$CO_2^+ + e \rightarrow CO + O$	$(Te/300)^{-0.5} \times 3.8 \times 10^{-7}$
A2	$O^+ + e \rightarrow O + h\nu$	$(Te/300)^{-0.5} \times 3.4 \times 10^{-12}$
A3	$CO^+ + e \rightarrow CO$	$(Te/300)^{-0.53} \times 6.5 \times 10^{-7}$
A4	$He^+ + e \rightarrow He + h\nu$	$(Te/300)^{-0.5} \times 4.4 \times 10^{-12}$
A5	$N^+ + e \rightarrow N + h\nu$	$(Te/300)^{-0.5} \times 3.3 \times 10^{-12}$
A6	$N_2^+ + e \rightarrow N + N$	$(Te/300)^{-0.5} \times 2.5 \times 10^{-7}$
A7	$H^+ + e \rightarrow H + h\nu$	$(Te/300)^{-0.5} \times 4.4 \times 10^{-12}$
A8	$O_2^+ + e \rightarrow O + O$	$(Te/300)^{-0.73} \times 2.0 \times 10^{-7}$

variation of charged particles in a planetary ionosphere is governed by the continuity equation

$$\frac{\partial N_e}{\partial t} = q - L - \nabla(N_e V) \tag{4}$$

a steady state situation ($\partial N_e/\partial t = 0$) can often be assumed[14]. However, during sunrise and sunset or during rapidly varying situations such as a solar eclipse for which density variations with time is fast, the $\partial N_e/\partial t$ cannot be assumed to be zero. The exact nature of transport processes is also not known. Therefore, in the present study, we have considered chemical equilibrium ($q = L$), when production and loss processes are predominant. The main ionic reactions which are responsible for the productions and losses of fresh ions have been discussed. For Venusian neutral atmosphere, we have taken height profiles of seven neutral species CO_2, O, CO, He, N, N_2 and H. The production and loss process are very much complex processes. Therefore, we are only considering major possible reactions for production and loss of corresponding ionic species and have obtained the steady state ion densities of each of the ions with the help of ion-neutral reactions rates and dissociative recombination rates. We have computed the steady state of each of the ion density cm^{-3} with the help of continuity equation for chemical equilibrium condition. For each of the major ions, we write[8]

$$(He^+) = q_{He}/[A4(N_e) + [R12 + R13 + R14](CO_2) + R15(CO) + [R16 + R17](N_2)] \tag{5}$$

$$(N_2^+) = [q_{N_2} + R17(He^+)(N_2)]/[A6(N_e) + R5(CO) + R6(CO_2) + R7(O)] \tag{6}$$

$$(N^+) = [q_N + R16(He^+)(N_2)]/[A5(N_e) + R10(CO) + R11(CO_2)] \tag{7}$$

$$(CO^+) = [q_{CO} + R5(N_2^+)(CO) + R10(N^+)(CO) + R12(He^+)(CO_2) + R15(He^+)(CO)]/[A3(N_e) + R3(O) + R4(CO_2)] \tag{8}$$

$$(O^+) = [q_O + R3(CO^+)(O) + R7(N_2^+)(O) + R14(He^+)(CO_2) + R18(H^+)(O)]/[A2(N_e) + R8(CO_2) + R9(H)] \tag{9}$$

$$(CO_2^+) = [q_{CO_2} + R4(CO^+)(CO_2) + R6(N_2^+)(CO_2) + R11(N^+)(CO_2) + R13(He^+)(CO_2)]/[A1(N_e) + R1(O) + R2(H)] \tag{10}$$

$$(H^+) = [q_H + R9(O^+)(H) + R2(CO^+)(H)]/[A7(N_e) + R18(O)] \tag{11}$$

$$(O^+) = [R1(CO_2^+)(O) + R8(O^+)(CO_2)]/A8(N_e) \tag{12}$$

The total number of positive ions in the ionosphere is written as

$$(N_i^+)_{Total} = (CO_2^+) + (O^+) + (CO^+) + (He^+) + (N^+) + (N_2^+) + (H^+) + (O_2^+).$$

Ignoring the total concentration of negative ions and considering charge neutrality of the Venus ionosphere, we write $\sum_i (N_i^+) = N_e$.

In order to solve equations (5)–(12) for ions and electron density rigorously, we have adopted a simpler iterative method. In this method, we started with a trial solution for electron density N_e' and taking neutral atmospheric model, the relevant rate coefficients and production rates, the number densities of ions are computed. The value of the sum of all the ion densities, $\sum_i N_i$ is compared with the adopted value N_e. If there is a difference between $\sum N_i$ and N_e', the whole procedure is repeated by taking another trial value of N_e'. This reiteration is continued until the trial solution $N_e' = \sum N_i$ is obtained within the limits of desired accuracy.

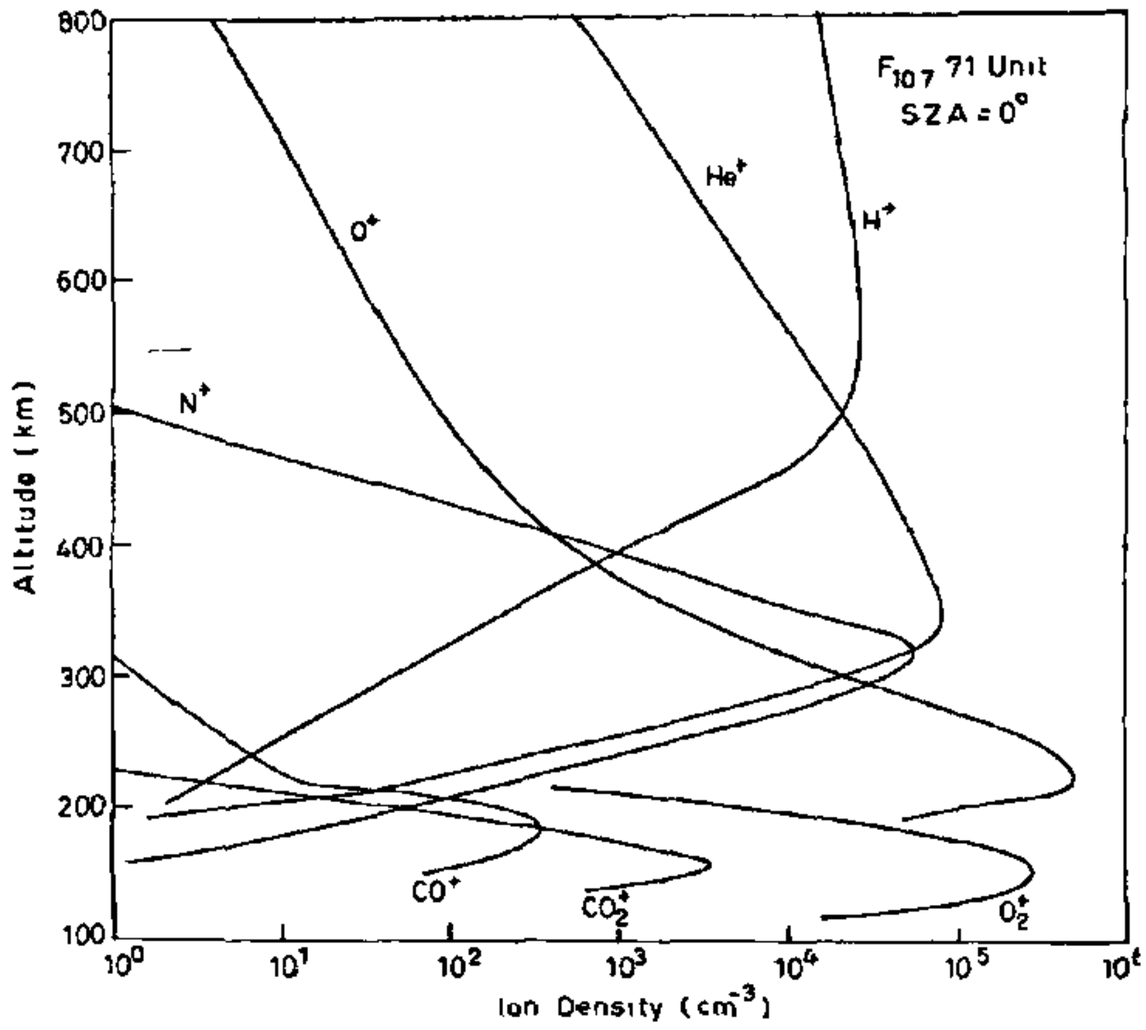

Figure 4. Differential equilibrium ion density profiles in the absence of vertical transport

Cosmic-ray ionization

We have considered the extremely relativistic and non-relativistic heavy cosmic-ray particles say protons and muons. The general formula for energy attenuation of these particles for inelastic collisions is written as[15]

$$(dE/dX)_{Coll} = -NZ\Phi_0 \frac{3}{4}\frac{z^2}{\beta^2}\left[\mathrm{Log}\frac{2\mu\beta^2 W_m}{I^2 Z^2 (1-\beta^2)} - 2\beta^2\right],$$

where N is the number of atoms per cm^3, ϕ_0 the $(8\pi/3)r_0^2$ unit cross-section, μ the rest energy of electron, z the charge of primary particle in terms of electronic charge, Z the atomic number, I the average ionization energy 11.5 eV, W_m the maximum energy that can be transferred to a free electron by the primary.

As a result of this energy input, the electron–ion production rate is written as:

$$q(h) = 2\pi / Q \int (dE/dh)_{Coll}\, n(h, E)\, dE$$

Taking different spectral features of the incident heavy protons and muons, we have computed the ionization profiles which are shown in Figure 7. We find that the muon flux penetrates much deeper into the Venus atmosphere where Venus cloud deck is in active circulation process. The charging of the Venus cloud is likely to play an important role in the electrodynamical state of the Venus' lower atmosphere.

Results and discussion

The electron–ion pair production rate computed earlier gives the instantaneous picture of the plasma production by solar photoionization processes. The electron–ion pairs produced in the ionosphere undergo various types of reactions with neutrals and the other ionic species. The variation of each of the ionic density is governed by the continuity equation which accounts for the losses and their kinetic production. The reactions responsible for localized production and losses give rise to steady state distributions of ion density in the ionosphere and the sum of all the ions equal the neutralizing electron density. The computation for each of the species has been carried out by taking relevant reactions and their reaction rates. The differential steady state ion densities profiles are shown in Figure 4. This figure is an example of many ion density profiles which have been computed for sub-solar and for low solar activity periods. We find that the ion density peaks at lower altitudes are formed by O_2^+ and O^+ ions. At higher altitudes, the He^+ and H^+ are found to be the dominant ions and are seen to be fairly large compared to O^+ ion density distributions. This is somewhat larger than the theoretically computed results reported by other workers[1, 16–19]. This difference may be partly due to the extrapolated neutral gas densities for higher altitudes used in this computation. The temperature and pressure dependence of reaction rates appropriate for use at higher altitudes are also not known. However, the nature of these ion density profiles at lower altitudes is quite consistent with the similar calculation reported by other workers[1, 16–19]. For the sake of comparison, we show the *in situ* measured ion densities for one subsolar season covering PVO orbits 170–203. These result for four of the major ions shown in Figure 5. The peaks of ion densities are found to be as follows:

Ion species	Ion density	Altitude
CO_2^+	$> 10^4$ cm^{-3}	175 km
O_2^+	3×10^5 cm^{-3}	175 km
O^+	$\sim 10^5$ cm^{-3}	> 200 km
H^+	$\sim 2 \times 10^2$ cm^{-3}	> 250 km

In Figure 5 dotted lines indicate the envelope corresponding to the lower values, medium values and upper values. The peaks at lower altitudes and the density of ions at lower altitudes show a fairly good similarity and comparison. However, the comparison at higher altitudes is not very promising and this discrepancy is seen to increase for lighter ions. We have used the detailed computations of ion densities to compute the electron density profiles corresponding to three solar activity

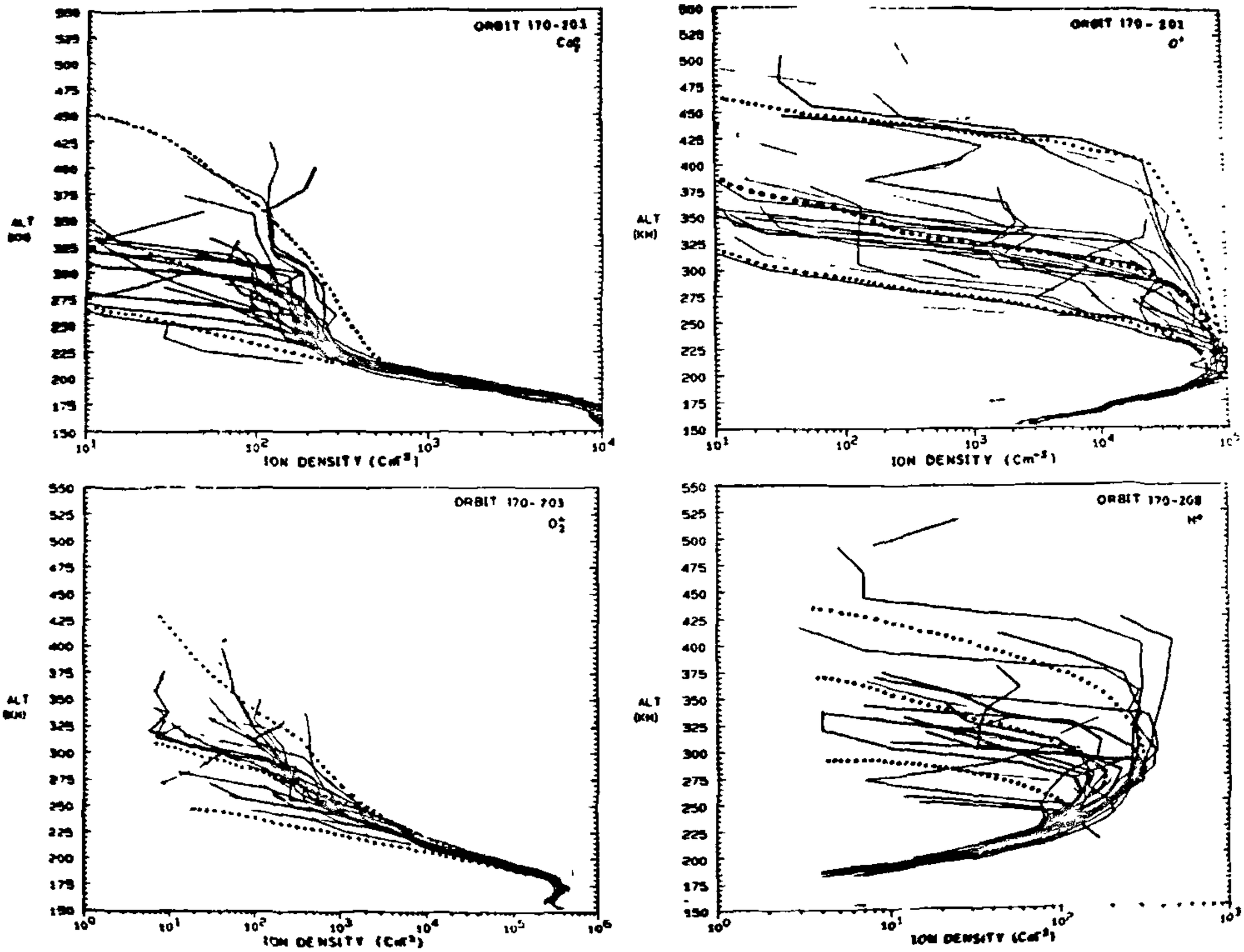

Figure 5. *In-situ* measured CO_2^+, O_2^+, O^+ and H^+ density profiles for PVO orbits 170–203. The three most probable dotted envelops showing upper, lower and medium values are shown for the sake of comparison with computed ion density profiles of Figure 4

indices of $F_{10.7} = 68$, 206 and 246. These electron densities are shown by the dashed lines in Figure 6. These profiles are of steady state electron densities which do not account for the effect of plasma transport. The primary forces governing the plasma transport are not yet precisely known, therefore, no concrete theoretical model for plasma transport processes in the Venus ionosphere is yet available. It is quite likely that the *in situ* measured electron density profiles are drastically modified by the plasma transport which is prevalent at the time of measurement and in the region of measurement. It seems that no meaningful comparison of *in situ* measured electron density and theoretically computed electron density can be made, in the light of some of these limitations. Such a comparison could only be meaningful at lowest altitudes where the effect of the vertical plasma transport is relatively small and ions are heavy. Further, the *in situ* measured electron density at higher altitudes may change with solar wind dynamic pressure and the solar activity index. These considerations do not allow one-to-one comparison and correspondence between theoretically computed and *in situ* measured electron density especially at higher altitudes. Figure 6 shows the envelope of the *in situ* measured OETP electron density data for the orbits 160–220. The U, M and L designate the maximum, medium and lower values of the electron densities. The comparison of calculated and measured electron density shows a drastic change at higher altitudes. We find that the *in situ* measured N_e and computed N_e are of the same order of magnitude at altitudes below 250 km. However, a large difference in theoretically computed and *in situ* data is seen. The exact source of such a large difference is not yet exactly

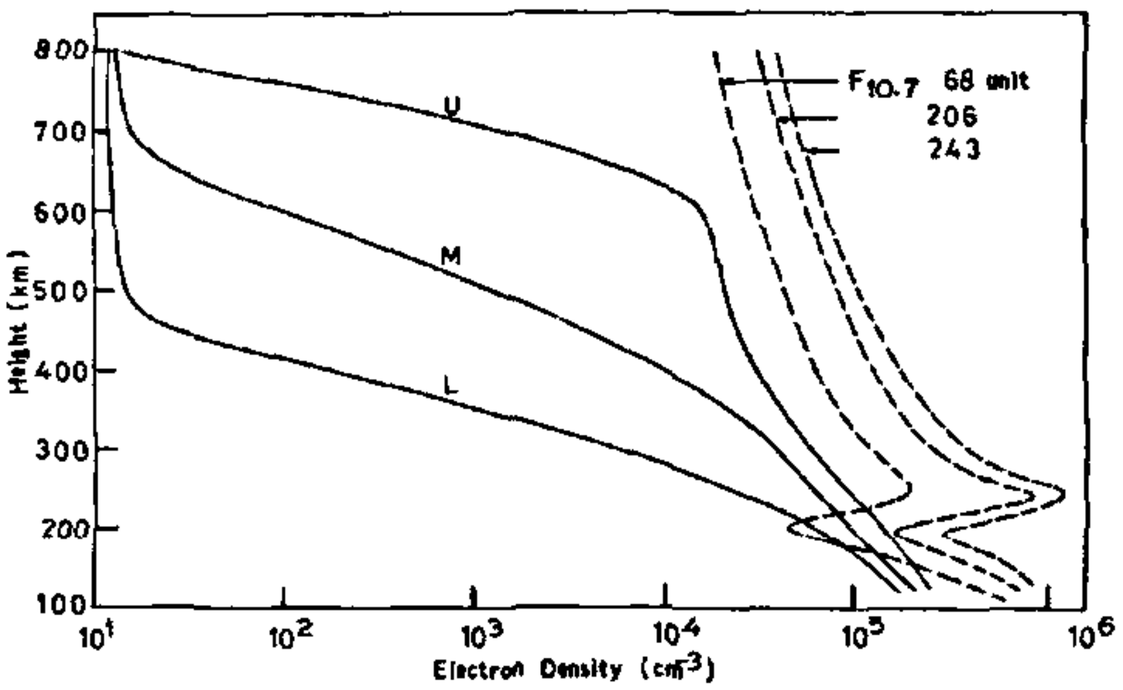

Figure 6. *In-situ* measured OETP Venus electron density profiles corresponding to lower, medium and upper ionopause during PVO orbits 160--220 (solid line) The theoretically computed electron density profiles for three solar activity conditions (dashed lines)

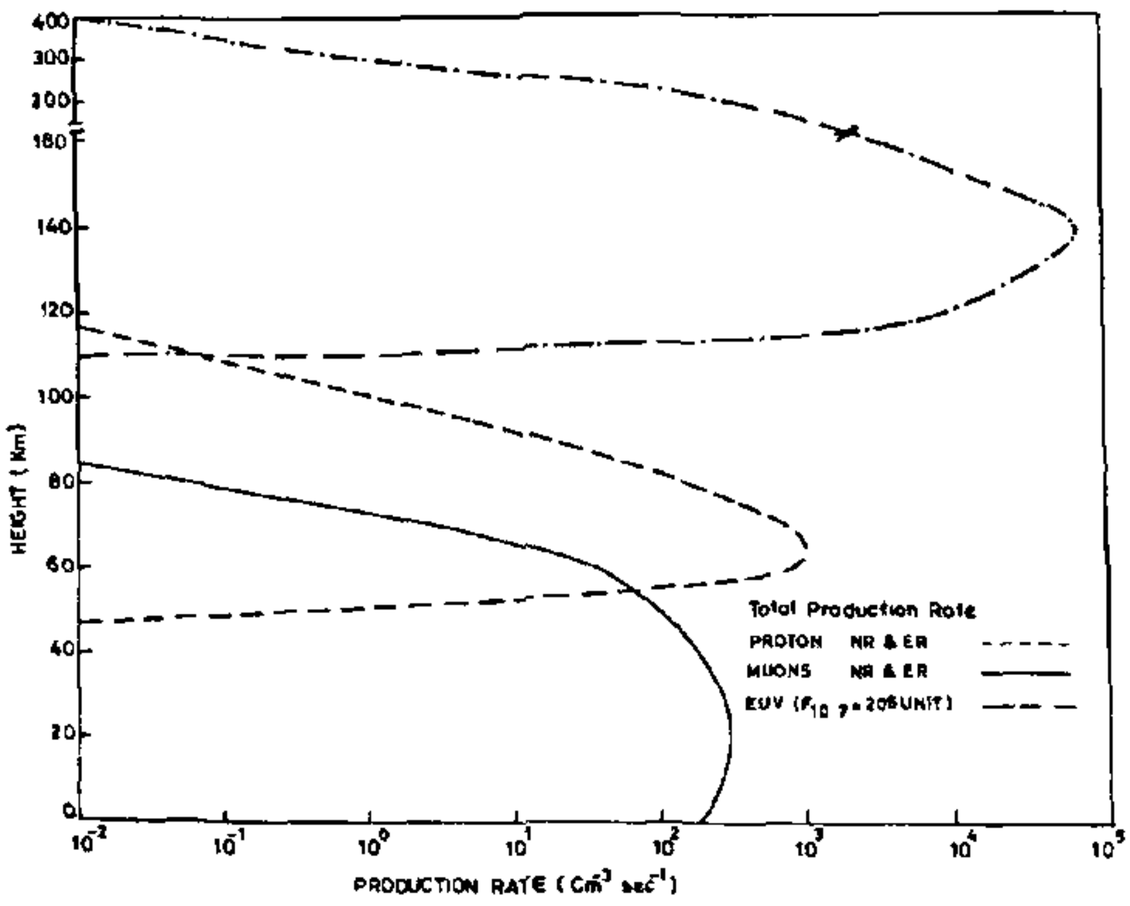

Figure 7. The electron–ion pair production rate produced by the cosmic-ray attenuation and decay processes in the Venus lower atmosphere

known. However, this difference may be attributed to likely errors in measurements and are partly affected by plasma transport processes, that have not been accounted for in this theoretical modelling.

The ionization in the lower ionosphere has not been measured by *in situ* devices. The photoionization also does not penetrate into the denser atmosphere of Venus to produce significant ionization. The dense atmosphere of Venus works a good stopper to relativistic and extreme relativistic protons and muons. A sample computation of cosmic-ray ionization has been carried out and the electron-ion production rate profiles have been obtained which shown in Figure 7. We find that the extreme relativistic protons and muons penetrate to much lower altitudes. The ion densities affected by cloud dynamics may result into charging the Venus clouds and consequent charge separation resulting in cloud lightning discharges generating broadband electromagnetic spectrum as measured by probes aboard PVO[20–23] and recently reported high frequency measurements during Galileo's flyby of nightside of Venus[24, 25]

Concluding remarks

The photoionization and ion-chemistry of the Venus ionosphere is almost similar to that of Earth's ionosphere. The solar wind interaction with Venus ionosphere is predominantly different from that of Earth's ionosphere. This difference basically arises because of the weak magnetic field of the Venus and relatively large temperature of the Venus atmosphere. The solar wind is mass-loaded and forms the ionopause at lower altitudes. Therefore, theoretically computed and *in situ* measured electron and ion densities during daytime can be compared only at lower altitudes. At higher altitudes theoretical and experimental values are found to change significantly. This difference is attributed to the control by the solar wind dynamic pressure and the vertical transport set in by the impact of solar wind. With changing solar wind dynamic pressure the ionopause altitude is found to oscillate. The ionopause feature of Venus is therefore, significantly different from that of Earth's magnetopause. The plasma transport processes are much more effective at higher altitudes. This may affect the measurement by different probes as has been discussed by Knudsen *et al.*[26] in many of their papers. It is shown that the lower part of the Venus atmosphere is ionized by the extremely relativistic proton and muon fluxes that may play an important role in understanding the charge separation and the production of cloud-to-cloud electrical discharges.

1 Schunk, R W and Nagy, A F, *Rev Geophys Space Phys*, 1980, 18, 813–852
2 Brace, L. H, Taylor, H A Jr, Gombosi, T I, Kliore, A J, Knudsen, W C and Nagy, A F, *Venus* Arizona Univ Press, Tucson, 1983, pp 779–840
3 Nagy, A F, Cravens, T E. and Gombosi, T I, *Venus*, Arizona Univ Press, Tucson, 1983, pp 841–872
4 Torr, M R, Torr, D G, Ong, R A and Hinteregger, H E, *Geophys Res Lett*, 1979, 6, 771–774
5 Marr, G V, *Photoionization Process in Gases*, Academic Press, New York, 1969
6 West, J B, *Proc R Soc (London)*, 1967, A349 397 421
7 Henry, J W and McElroy, M B, in *Atmospheres of Venus and Mars*, Gordon and Breach, 1968, pp 251–285
8 Cloutier, P A and Daniel, R E Jr, *Planet Space Sci* 1979 27, 1111–1112
9 Kliore, A J, Moroz, V I and Keating, G M, *Adv Space Res*, 1985, 5(11), 1–269
10 Hinteregger, H E, *Adv Space Res*, 1981, 1(12) 39 52
11 Wilkes, M V, *Proc Phys Soc (London)* 1951 B76 301 308
12 Smith, E J and Smith C, *J Geophys Res* 1972 77 3592–3597
13 Fox, J L, *Icarus* 1982, 51, 248 260

14 Bauer, S J , *Physics of Planetary Ionospheres*, Springer-Verlag, Berlin, 1973
15 Heitler, W , *The Quantum Theory of Radiation*, Clarendon Press, Oxford, 1954, pp 368
16 Chen, R H , PhD thesis, The University of Michigan, Ann Arbor, 1977, USA
17 Chen, R H and Nagy, A F , *J Geophys Res* , 1978, **83**, 1133–1140
18 Nagy, A F , Cravens, T E , Chen, R. H , Taylor, H A Jr , Brace, L. H. and Brinton, H C , *J Geophys Res* , 1980, **85**, 7795–7801
19 Shinagawa, H , PhD thesis, The University of Michigan, Ann Arbor, USA, 1987
20. Taylor, W W L , Scarf, F L , Russell, C T and Brace, L H , *Nature*, 1979, **279**, 614–616
21 Ksanfomality, L. V , *Nature*, 1980, **284**, 244–246
22 Scarf, F. L and Russell, C T , *Geophys Res Lett* , 1983 **12**, 1191–1195
23 Singh, R N and Russell, C T , *Geophys Res Lett* , 1986, **13**, 1051–1054
24 Kerr, R. A , *Science*, 1991, **253**, 1492
25 Gurnett, D A , Kurth, W S , Roux, A , Gendrin, R , Kennel, C F. and Bolton, S J , *Science*, 1991, **253**, 1522–1525
26. Knudsen, W C , Spenner, K , Miller, K L and Novak, V , *J Geophys. Res* , 1980, **85**, 7803–7810